

Shape Reconstruction of Three Dimensional Conducting Objects Using Opposition-Based Differential Evolution

Mojtaba Maddahali¹, Ahad Tavakoli¹, and Mojtaba Dehmollaian²

¹Department of Electrical Engineering
Amirkabir University of Technology, Tehran, 15875-4413, Iran
tavakoli@aut.ac.ir, maddahali@aut.ac.ir

²School of Electrical and Computer Engineering
University of Tehran, Tehran, 14395-515, Iran
m.dehmollaian@ece.ut.ac.ir

Abstract — In this paper, shape reconstruction of three dimensional conducting objects using radar cross section (RCS) of the scatterer and opposition-based differential evolution is investigated. The shape of the scatterer is modeled with nonuniform rational B-spline (NURBS) surfaces composed of more than one Bezier patches. NURBS are piecewise polynomial with unknown coefficients that are determined in the procedure of shape reconstruction. Opposition-based differential evolution (ODE) is then employed as an optimization tool to find the unknown coefficients. Physical optics approximation is used to predict RCS of the large conducting scatterer in various directions and at multiple frequencies. The effect of noise is also considered in the inverse process.

Index Terms — Inverse scattering, NURBS modeling, opposition-based differential evolution, physical optics approximation.

I. INTRODUCTION

The objective of inverse scattering methods is to discover features of an object by means of the electromagnetic (EM) scattered field. These methods have several applications such as nondestructive testing, biomedical imaging, and ground-penetrating radars. The complexity encountered in inverse scattering is mostly due to ill-posed and nonlinear problems. Mathematical algorithms of inverse scattering problems are mostly categorized into the time-domain or the frequency-domain solutions. The time-reversal method is an example of time-domain solutions [1]. Optimization methods are mostly utilized in widely used frequency-domain approaches. Optimization methods are commonly used for reconstruction of two dimensional conducting and dielectric objects [2-5]. In [2], the shape of the scatterer is modeled with the cubic B-spline curves. These curves are piecewise polynomial where

their coefficients are determined by control points. The control points are found such that a specific measure of difference between reconstructed and original scattered fields is minimized. This approach could be generalized to three dimensional problems. In this case, the structure is modeled with non-uniform rational B-spline (NURBS) surfaces. NURBS are also piecewise polynomials where their coefficients are defined by a set of control points and associated weights. For computational purposes, NURBS surfaces are decomposed into Bezier surfaces. These surfaces are also piecewise polynomials. In [6], a NURBS surface composed of only one Bezier patch is considered and genetic algorithm (GA) is used to reconstruct the shape of a three dimensional conducting object.

Generally, NURBS surfaces have a complex geometry and are composed of more than one Bezier surface. This paper tries to reconstruct a more complex structure composed of more than one Bezier surface. The geometrical continuity of the surfaces complicates the reconstruction approach. The proposed algorithm is based on opposition-based differential evolution (ODE) as an optimization tool, because unlike GA, the ODE is simple to implement; it does not require coding and decoding of population members. In each iteration of the optimization algorithm, RCS of the reconstructed conducting body is calculated using physical optics (PO) approximation. The paper is organized as follow. Section II presents a brief review of NURBS modeling. Computation of PO integral is discussed in Section III. The inverse problem is discussed in Section IV. Some simulation results are presented in Section V. Concluding remarks are given in Section VI.

II. GEOMETRIC DESCRIPTION OF THE BODIES

In this paper, non-uniform rational B-spline surfaces are used for geometric modeling of the bodies.

The main reason for this choice is that a small amount of information is needed for accurate representation of complex objects. NURBS surfaces are specified with a set of control points, associated weights, and knot vectors. A NURBS surface is expanded as a set of Bezier patches. Geometrical parameter calculation of Bezier patches is easier than the NURBS surfaces. In the following, we discuss the concept of rational Bezier curves and then extend it to the three-dimensional surfaces. Rational Bezier curves could be formulated as follows [7]:

$$\vec{r}(u) = \frac{\sum_{i=0}^m w_i \vec{b}_i B_i^m(u)}{\sum_{i=0}^m w_i B_i^m(u)}, \quad (1)$$

where $\vec{b}_i \in R^3$, $i=0, \dots, m$, are the control points, $w_i \in R$, $i=0, \dots, m$, are the associated weights, the integer m is the curve degree, and $B_i^m(u)$, $i=0, \dots, m$, are the Bernstein polynomials given by:

$$B_i^m(u) = \frac{m!}{i!(m-i)!} u^i (1-u)^{m-i}, \quad 0 \leq u \leq 1, \quad (2)$$

u is a parameter between zero and one that shapes the curve. When these control points move through space on another Bezier curve, a Bezier surface is formed. The resultant surface could be formulated as follows:

$$\vec{r}(u, v) = \frac{\sum_{i=0}^m \sum_{j=0}^n w_{ij} \vec{b}_{ij} B_i^m(u) B_j^n(v)}{\sum_{i=0}^m \sum_{j=0}^n w_{ij} B_i^m(u) B_j^n(v)}, \quad (3)$$

where $\vec{b}_{ij} \in R^3$, $i=0, \dots, m$, $j=0, \dots, n$, are the control points, $w_{ij} \in R$, $i=0, \dots, m$, $j=0, \dots, n$, are the associated weights, and the integers m and n are degrees of the surface. Similar to u , v is a parameter between zero and one that shapes the other dimension of the surface. When a set of Bezier surfaces are connected by a specific continuity rule, a B-spline surface is formed. The resulting B-spline surface has an appealing property of local control ability [7]. A B-spline surface can be expanded as a linear combination of B-spline basis functions [9].

III. PHYSICAL OPTICS

When the dimensions of the conducting object are large compared to the wavelength, the backscattering electric field is specified by [9]:

$$\vec{E}_s(r) = -\frac{j}{\lambda} \frac{\exp^{-jk_0 r}}{r} (\hat{k} \cdot \vec{I}) \vec{E}_0, \quad \vec{I} = \int n(r') \exp^{j2\hat{k} \cdot r'} ds', \quad (4)$$

where λ is the operating wavelength, \vec{E}_0 is the polarization of the incident field, \hat{k} is the wave vector, \vec{r}' is the position vector, ds' is the differential element

of the surface, \hat{n} is the normal vector at the surface point, k_0 is the wave number, and \vec{I} is the physical optics integral. For a Bezier surface, \vec{I} is written as follows:

$$\vec{I} = \int_{u=0}^{u=1} \int_{v=0}^{v=1} g(u, v) \exp[jkf(u, v)] dudv, \quad (5)$$

where

$$\vec{g}(u, v) = \vec{r}_u \times \vec{r}_v, \quad f(u, v) = 2\vec{k} \cdot \vec{r}'(u, v). \quad (6)$$

Any surface can be formed with composition of three kinds of Bezier surfaces, (a) singly curved, (b) doubly curved, and (c) plane patch. PO integral can be evaluated for these kinds of surfaces as explained in continue.

A. Singly curved surfaces

When the degree of a Bezier surface is equal to one, then a singly curved surface is formed as shown in Fig. 1 (a). In other words, this surface is formed when a curve moves on a straight line in space. Suppose that the surface is linear along parameter v , then the phase term in PO integral can be written as follows:

$$f(u, v) = f_0(u) + v f_1(u) = 2\vec{k} \cdot \vec{r}_0(u) + v 2\vec{k} \cdot \vec{r}_1(u), \quad (7)$$

thus, the PO integral is

$$\vec{I} = \int_{u=0}^{u=1} \exp[jkf_0(u)] \int_{v=0}^{v=1} \vec{g}(u, v) \exp[jkvf_1(u)] dudv. \quad (8)$$

Integration with respect to the parameter v can be computed by expanding $g(u, v)$ in Taylor series around $v_0 = 0.5$ and then calculating the integral of each term in the series analytically, then we have,

$$\vec{I} = \int_{u=0}^{u=1} \exp[jkf_0(u)] G(u), \quad (9)$$

where $G(u)$ is

$$G(u) = \sum_{n=0}^{n=N} \sum_{k=n}^N \frac{g^k(u, v_0) (v_0)^{k-n}}{(k-n)! n!} A_n(u), \quad (10)$$

and

$$A_n(u) = \int_{v=0}^{v=1} v^n \exp[jkf_1(u)] dv = \frac{n!}{-jkf_1^{n+1}(u)} - \sum_{i=0}^n \frac{n! \exp[jkf_1(u)]}{(n-i)! [-jkf_1(u)]^{i+1}}. \quad (11)$$

Integration with respect to the parameter u can be evaluated via a trapezoidal numerical method. In some references, this integral is computed with stationary phase method [8-10]; however our simulations show that numerical method is more accurate.

B. Doubly curved surfaces

When both degrees of a Bezier surface is greater than one, a doubly curved surface is formed as shown in Fig. 1 (b). In this case, currents near the certain critical points produce the main contribution of the scattered field. There are three kinds of critical points: stationary phase points, boundary points, and vertex

points as shown in Fig. 2. The phase term of the integrand is expanded in Taylor series around the critical points and then physical optics integral is easily calculated. This method is explained in [8-10].

C. Plane patches

When both degrees are equal to one, a plane patch is formed as shown in Fig. 1 (c). For plane patch, PO integral can be evaluated using Gordon method [11].

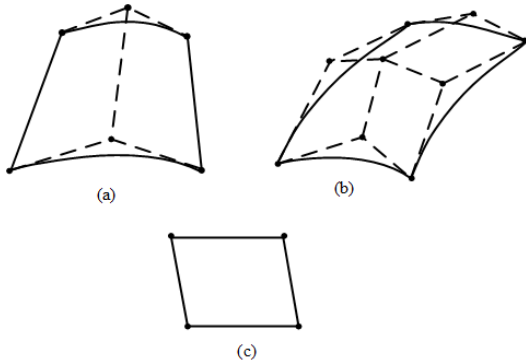


Fig. 1. Three kinds of Bezier surfaces and their control points: (a) singly curved surface, (b) doubly curved surface, and (c) plane patch [8].

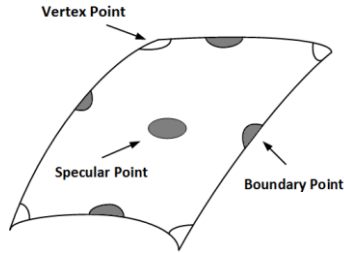


Fig. 2. critical points over the Bezier surface [5].

IV. INVERSE SCATTERING

In the inverse scattering procedure, the control points of the rational spline surface are optimally located such that the RCS of the reconstructed scatterer in multiple directions and at several frequencies approaches the RCS of the original scatterer. Here, the shape of the scatterer is approximated by a degree- n surface that is constructed by rational spline curves (Fig. 3). The shape of these curves and the distance between them are determined by an optimization algorithm. Therefore, arbitrary objects can be reconstructed. Compared to the reference [6], an exact algorithm for reconstruction is presented here, and some complex objects are rebuilt as well. In addition, in this case, other issues such as the effect of the shadowing of a surface by another surface, is taken into consideration by the authors while nothing is concerned in reference [6] regarding this effect.

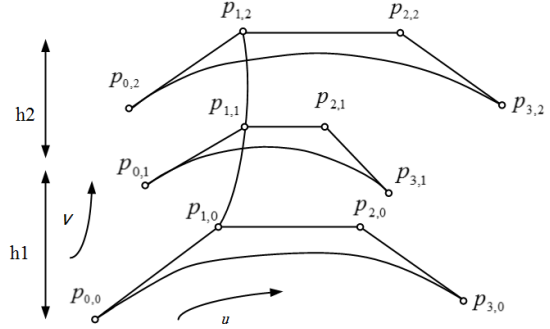


Fig. 3. Control points of the object.

A. Optimization algorithm

The opposition-based differential evolution is our optimization approach as follows. If the problem has D unknown parameters, then NP parameter vectors of D -dimension are produced in the first step [12]:

$$x_{i,j}, \quad i = 1, \dots, NP. \quad (12)$$

Then, the opposite population is calculated by:

$$ox_{i,j} = a_j + b_j - x_{i,j}, \quad (13)$$

where a_j and b_j are the lower and upper bounds of the j^{th} dimension of the parameter vector respectively. If the cost function of $ox_{i,j}$ is lower than $x_{i,j}$, then $x_{i,j}$ is replaced by $ox_{i,j}$. According to probability principles, this happens 50% of the time. In the second step, a mutant vector is produced for each target vector as:

$$v_i^{G+1} = x_{r_1}^G + F \cdot (x_{r_2}^G - x_{r_3}^G), \quad (14)$$

where G is the generation index and r_1, r_2, r_3 are three mutually different integers that also differ from target index i . F is also the mutant constant that is usually taken to be 0.8. Next, from the combination of the mutant vector and the target vector, the trial vector is produced:

$$u_i^{G+1} = (u_{i1}^{G+1}, u_{i2}^{G+1}, \dots, u_{Di}^{G+1}), \quad (15)$$

where

$$u_{ji,G+1} = \begin{cases} v_{ji}^{G+1} & \text{if } h_j \leq H \text{ or } j = l \\ x_{ji}^{G+1} & \text{if } h_j > H \text{ and } j \neq l \end{cases} \quad (16)$$

In this equation, h_j is a random number in the interval $[0,1]$, $H \in (0,1)$ is a crossover constant selected by the user, and l is a random integer $\in [1,2,\dots,D]$. If the cost function of u_i^{G+1} is smaller than x_i^{G+1} , then x_i^{G+1} is replaced by the trial vector. Similarly, opposite of the current population is generated by:

$$ox_{i,j}^G = \text{MIN}_j^G + \text{MAX}_j^G - x_{i,j}^G, \quad (17)$$

where MIN_j^G and MAX_j^G are the minimum and maximum of j^{th} dimension in the current population. Now, a random number between $[0,1]$ is generated and

if it is lower than the preselected jumping rate J_r , then $x_{i,j}^G$ is compared with $ox_{i,j}^G$ and the one with a lower cost function is selected as the member of the current population. Here, the selected parameters of the opposition-based differential evolution are listed in Table 1.

B. RCS based cost function

The cost function for this optimization is defined as:

$$f(p) = \frac{\sum_{\omega} \sum_{\theta} \sum_{\phi} |\sigma_{\theta\phi\omega}^{true} - \sigma_{\theta\phi\omega}^{rec}|}{\sum_{\omega} \sum_{\theta} \sum_{\phi} |\sigma_{\theta\phi\omega}^{true}|}, \quad (18)$$

where $\sigma_{\theta\phi\omega}^{true}$ and $\sigma_{\theta\phi\omega}^{rec}$ are radar-cross sections of the original and the reconstructed scatterer respectively. The cost function is minimized to find the location of control points, p and the distance between curves. For considering the noise effect, the original RCS is modified as follows [6]:

$$\sigma_{\theta,\phi,\omega}^n = \sigma_{\theta,\phi,\omega} + \sqrt{\sigma_{\theta,\phi,\omega}^2} \times (NL) \times (rand). \quad (19)$$

In this equation, $\sqrt{\sigma_{\theta,\phi,\omega}^2}$ is the rms of the original RCS, NL is the noise level, and $rand$ is a random number picked from the interval [0,1]. In this paper, the radar cross section of the scatterer is used in the cost function, so that the phase of the scattered field is not taken into account, and the transmission of the object is obtained.

V. NUMERICAL RESULTS

For the first example, the reconstruction of perfectly conducting cone modeled with one NURBS surface composed of three Bezier surfaces is presented. The cone has the height of 1m and the bottom radius of 1m and the top radius of 0.5m as shown in Fig. 4 (a). In the reconstruction procedure, the degree of the surface and weight coefficients are selected a-priori. In addition, we assume that the curvature of the surface is negative. It should be noted that the weight of control points and the degree of surface can also be considered as the optimization parameters; however, in this state, the volume of computations is enormous and it is not considered here as just a generalized method for complex structures was aimed. This cone is modeled with 6x2 control points. The scattered field is evaluated at 45 points that are uniformly located around the object at $\theta = 60^\circ, 75^\circ, 90^\circ$ and at frequencies of 0.4, 0.8, 1.2 GHz.

Figure 4 (b) displays the reconstructed cone. The average cost function for five simulations as a function of number of iterations are depicted in Fig. 4 (c). The RCS of the original and the reconstructed cones are presented

in Fig. 4 (d). A very good agreement between the original cone and the reconstructed cone is observed.

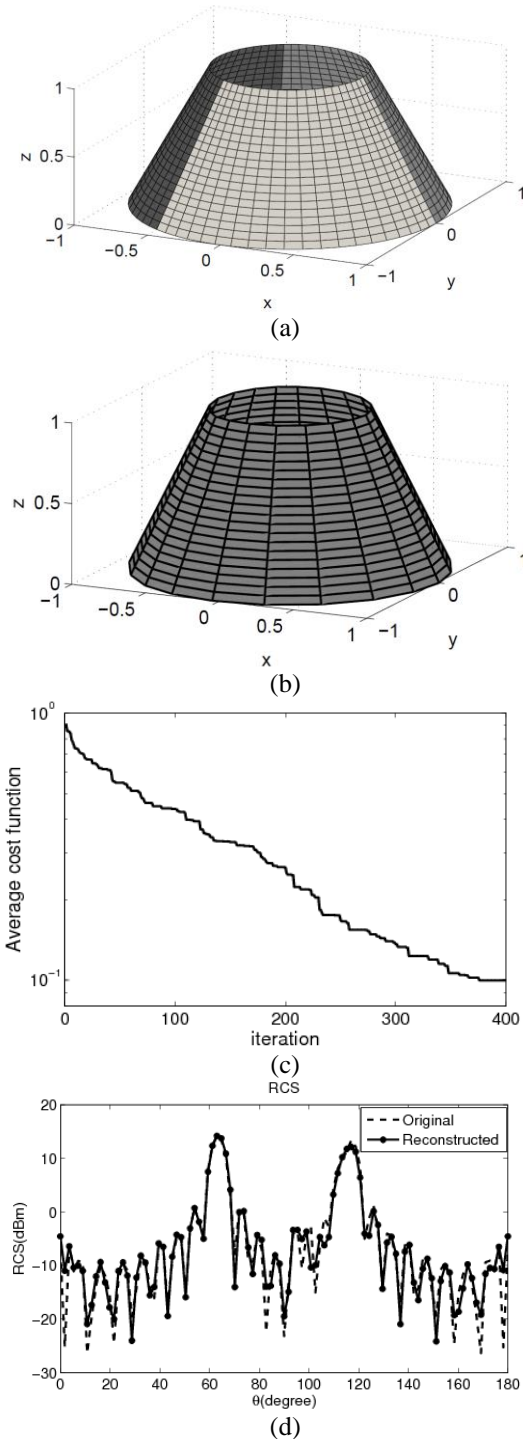


Fig. 4. (a) Original half cone, (b) reconstructed half cone, (c) average cost function, and (d) radar cross section of the original and the reconstructed cone at $f = 1.2\text{GHz}$ and $\phi = \pi/4$.

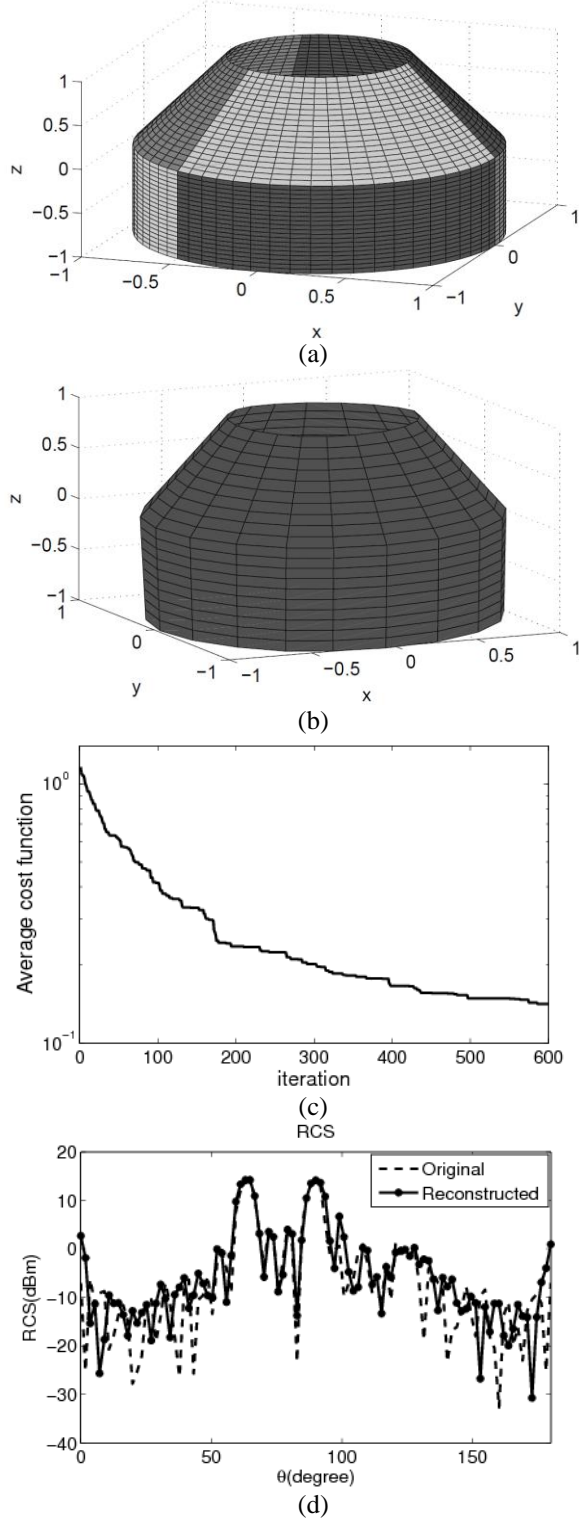


Fig. 5. (a) Original cone cylinder, (b) reconstructed cone cylinder, (c) average cost function, and (d) radar cross section of the original and the reconstructed cone-cylinder at $f = 1.2\text{GHz}$ and $\phi = \pi/4$.

Table 1: Opposition-based differential evolution parameters

Jumping Rate	Mutant Constant	Crossover Rate
0.5	0.8	0.5

To evaluate the accuracy of the reconstruction procedure, a shape error is defined as follow [6]:

$$RECP = \frac{1}{N_{vnet}} \left(\sum_{i=0}^m \sum_{j=0}^n \frac{\|\Delta^{0,1} p_{i,j}^{true} - \Delta^{0,1} p_{i,j}^{reco}\|^2}{\|\Delta^{0,1} p_{i,j}^{true}\|^2} + \frac{\|\Delta^{1,0} p_{i,j}^{true} - \Delta^{1,0} p_{i,j}^{reco}\|^2}{\|\Delta^{1,0} p_{i,j}^{true}\|^2} \right)^{1/2}, \quad (20)$$

where $N_{vnet} = 2mn + m + n$ is the number of elements in the vector net and $\|p_{i,j}\|$ is the Euclidean norm given by:

$$\|p_{i,j}\| = \sqrt{x_{i,j}^2 + y_{i,j}^2 + z_{i,j}^2}. \quad (21)$$

$\Delta^{0,1} p_{i,j}$ and $\Delta^{1,0} p_{i,j}$ are related to the control points as:

$$\Delta^{0,1} p_{i,j} = p_{i,j+1} - p_{i,j} \quad \Delta^{1,0} p_{i,j} = p_{i+1,j} - p_{i,j}. \quad (22)$$

In the simulation, the shape error for a half cone is calculated to be 0.04423. In the presence of a noise level of 10%, the shape error is 0.04725. For the second example, the reconstruction of perfectly conducting cone-cylinder modeled with one NURBS surface composed of six Bezier surfaces is presented. The cone-cylinder has the height of 1m for both the cone and the cylinder and radius of 1m at the bottom and 0.5m at the top. Similar to the previous example, Fig. 5 shows the target and the simulation results. Here, the shape error for cone-cylinder is calculated to be 0.071. In the presence of a noise level of 10%, the shape error is 0.1527. In the following, we can consider this issue for the reconstruction of buried objects by taking into account the effect of a background layer.

VI. CONCLUSION

In this paper, the PO approximation, the ODE algorithm, and NURBS modeling are used to reconstruct three-dimensional conducting objects. NURBS surface are used to model unknown scatterers by a minimum number of parameters. The reconstruction is done by applying the ODE algorithm as an optimization tool. Here, NURBS surfaces composed of more than one Bezier surface is reconstructed. A very good agreement between the original object and the reconstructed object is achieved.

REFERENCES

- [1] P. Kosmas and C. M. Rappaport, "Time reversal with the ftdt method for microwave breast cancer detection," *IEEE Transactions on Microwave Theory and Techniques*, vol. 53, no. 7, pp. 2317-

- 2323, July 2005.
- [2] I. T. Rekanos, "Shape reconstruction of a perfectly conducting scatterer using differential evolution and particle swarm optimization," *IEEE Trans. Geosci. Remote Sens.*, vol. 46, no. 7, pp. 1967-1974, July 2008.
- [3] A. Semnani, I. T. Rekanos, M. Kamyab, and M. Moghaddam, "Solving inverse scattering problems based on truncated cosine fourier and cubic b-spline expansions," *IEEE Trans. Antennas Propagat.*, vol. 60, no. 12, pp. 5914-5923, 2012.
- [4] C.-C. Chiu and R.-H. Yang, "Inverse scattering of biaxial cylinders," *Microwave and Optical Technology Letters*, vol. 9, no. 5, pp. 292-302, 1995.
- [5] I. T. Rekanos, "On-line inverse scattering of conducting cylinders using radial basis-function neural networks," *Microwave and Optical Technology Letters*, vol. 28, no. 6, pp. 378-380, 2001.
- [6] A. Saeedfar and K. Barkeshli, "Shape reconstruction of three-dimensional conducting curved plates using physical optics, nurbs modeling, and genetic algorithm," *IEEE Trans. Antennas Propagat.*, vol. 54, no. 9, pp. 2497-2507, Sept. 2006.
- [7] G. E. Farin, *Curves and Surfaces for Computer-Aided Geometric Design: A Practical Guide*. Number v. 1 in Computer Science and Scientific Computing. Academic Press, 1997.
- [8] J. Perez and M. F. Catedra, "Application of physical optics to the rcs computation of bodies modeled with nurbs surfaces," *IEEE Trans. Antennas Propagat.*, vol. 42, no. 10, pp. 1404-1411, Oct. 1994.
- [9] F. S. de Adana and O. Gutierrez, *Practical Applications of Asymptotic Techniques in Electromagnetics*. Artech House Electromagnetic Analysis Series. Artech House, 2010.
- [10] F. S. de Adana, I. G. Diego, O. G. Blanco, P. Lozano, and M. F. Catedra, "Method based on physical optics for the computation of the radar cross section including diffraction and double effects of metallic and absorbing bodies modeled with parametric surfaces," *IEEE Trans. Antennas Propagat.*, vol. 52, no. 12, pp. 3295-3303, Dec. 2004.
- [11] W. Gordon, "Far-field approximations to the kirchoff-Helmholtz representations of scattered fields," *IEEE Trans. Antennas Propagat.*, vol. 23, no. 4, pp. 590-592, July 1975.
- [12] S. Rahnamayan, H. R. Tizhoosh, and M. M. A. Salama, "Opposition-based differential evolution," *IEEE Transactions on Evolutionary Computation*, vol. 12, no. 1, pp. 64-79, Feb. 2008.



Mojtaba Maddah-ali was born in Isfahan, Iran, on December 5, 1987. He received B.Sc. degree in Electrical Engineering from Isfahan University of technology, Isfahan, Iran, in 2009, the M.Sc. degrees from the Amirkabir University of Technology, Tehran, Iran, in Electrical Engineering, in, 2013.



Ahad Tavakoli was born in Tehran, Iran, on March 8, 1959. He received the B.S. and M.S. degrees from the University of Kansas, Lawrence, and the Ph.D. degree from the University of Michigan, Ann Arbor, all in Electrical Engineering, in 1982, 1984, and 1991, respectively. He is currently a Professor in the Department of Electrical Engineering at Amirkabir University of Technology.



Mojtaba Dehmollaian was born in Iran in 1978. He received the B.S. and M.S. degrees in Electrical Engineering from the University of Tehran, Tehran, Iran, in 2000 and 2002, respectively. He received the M.S. degree in Applied Mathematics and Ph.D. degree in Electrical Engineering from the University of Michigan, Ann Arbor, in 2007. Currently, he is an Assistant Professor with the Department of Electrical and Computer Engineering, University of Tehran.